Toughness improvement of polyamide 11 assessed via quasistatic tensile tests on notched round bars

Lucien Laiarinandrasana, Guillaume Boisot, C. Fond, Gilles Hochstetter

TOUGHNESS IMPROVEMENT OF POLYAMIDE 11 ASSESSED VIA QUASI-STATIC TENSILE TESTS ON NOTCHED ROUND BARS

L. Laiarinandrasana [1)], G. Boisot [1,2)], C. Fond [2,3)], G. Hochstetter [4)]

[1)] MINES ParisTech, MAT-Centre des Matériaux, UMR CNRS 7633, B.P. 87, 91003 Evry Cedex, France
[2)] Institut Charles Sadron, CNRS-UPR 22, 23 Rue du Loess, BP 84047, 67034 Strasbourg Cedex, France
[3)] Institut de Mécanique des Fluides et des Solides, 2 Rue Boussingault, 67000 Strasbourg, France
[4)] ARKEMA Cerdato, Route du Rilsan, 27470 Serquigny, France

ABSTRACT

Toughening a polymeric material by adding rubber particles is a common technique used for glassy polymers and measured by means of Charpy or Izod impact tests. These latter are determined under dynamic conditions, thus at high strain rate or equivalently at very low temperature for polymeric materials.
This work is devoted to three grades of semi-crystalline PolyAmide 11 (PA11), used in a large number of engineering components. Service conditions are close to the glass transition temperature. Therefore, tests with quasi-static loading are expected to be more appropriate.
The aim of the study is to find a methodology allowing the quantification of toughness improvement. To this end, an experimental database was constituted. Three grades of PA11 were involved, that enable to analyze effects of: i) aging, ii) addition of a plasticizer iii) addition of rubber particles. Tensile tests were then carried out on notched round bars. Trends of load versus notch opening displacement curves are investigated. Longitudinal cross-sections on specimens issued from interrupted tests and fracture surfaces were examined in order to study deformation and damage mechanisms. An attempt is made to link toughness improvement to the increase in global fracture energy.

KEYWORDS

Rubber toughened polymers, Damage mechanics, Fracture mechanics, Finite element, Void growth, Cavitation, Polymer mechanics

INTRODUCTION

Toughness of polymeric materials is often characterized by the impact strength (from Charpy or Izod tests). They are dymamic tests at high strain rate level or equivalently at very low temperature below T_g (glassy polymers). When the service temperature is near or above T_g, impact strength may be inappropriate to determine the failure behaviour of the material. Indeed for fully ductile material, when the energy brought by the striker is less than the impact strength, the specimen will not break but only plastically deforms with a large deflection. It is essential to find a relevant parameter to predict the durability of structural polymers. Fracture mechanics approaches give an accurate definition of fracture toughness: the value at failure of the stress intensity factor for linear elastic fracture mechanics (LEFM: small scale yielding), or the value at crack initiation of the J-integral for elastic plastic fracture mechanics (EPFM: extended plastic zone). Comprehensive research has been carried out

for years on metallic materials concerning the equivalence between impact strength and fracture toughness [1-3]. On polymers, some attempts were made in this way but instead of the J-integral, the essential work of fracture was used. Requested plane strain conditions are difficult to fulfil.

This paper is devoted to three grades of Polyamide 11 (PA11). It follows the local approach to fracture methodology to assess the ductile failure of the materials. Indeed, for the PA11 of interest, mechanical tests were carried out on specific notched round tensile bars. Taking advantage of previous studies at EFC17 conference [4], one specimen geometry was chosen in order to analyze the effect of aging together with an amount of plasticizer and an addition of rubber toughening. Examinations of the void growth mechanisms were performed in order to identify the local failure criteria, depending on each material. The global mechanical response in terms of net stress versus axial displacement is analyzed. The mechanical parameters are studied and those that are relevant to predict the toughness improvement are highlighted.

MATERIAL, SPECIMEN AND TESTING

The materials of interest consist of 3 grades of Polyamide 11 (PA11) provided by ARKEMA: i) semi-crystalline neat PA11 (index of cristallinity = 25%); ii) “aged P40” is a plasticized PA11, aged for 7 days in pressurized water (pH7) at 140°C; iii) “aged P20R” is a plasticized, toughened by rubber particles (~250nm in diameter) PA11 aged for 7 days in pressurized water (pH7) at 140°C. For each material, some mecha nical characteristics were determined with the help of Dynamic Mechanical Analysis (DMA) tests, performed at a strain range of 0.5% at 5Hz.

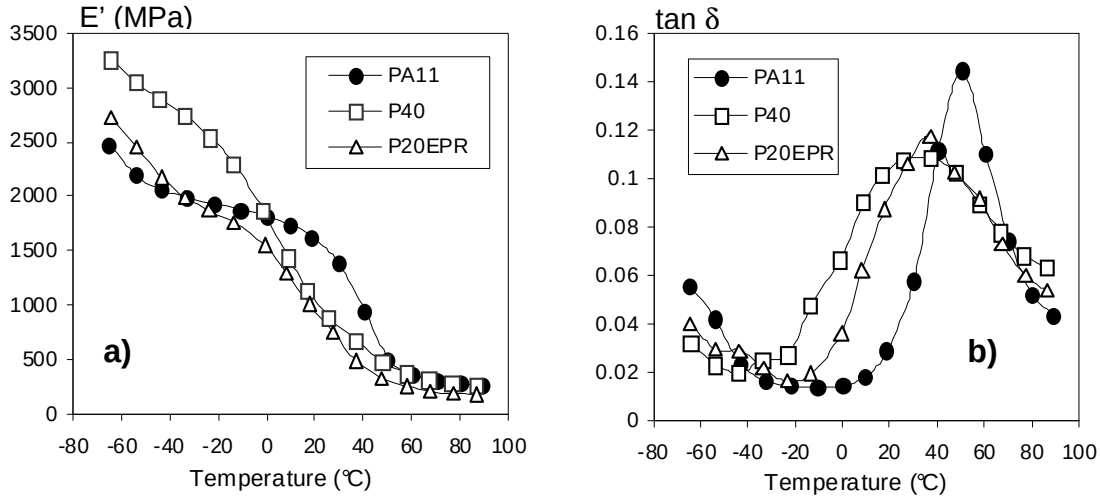

Figure 1: DMA results on all PA11 materials: a) storage moduli; b) evolution of tan δ with temperature

Figure 1 shows the evolution of the storage moduli and the damping coefficient tan δ. Further information concerning the materials is provided in Table 1.

The aim of the work is to investigate, on the PA11 material, the effects of plasticizer addition followed by aging (P40) as well as the effects of rubber toughening (aged P20R) based on data obtained on aged P40 material. Following the study of Boisot [4] concerning experimentation and damage modelling of PA11, where various kinds of specimens were

tested (smooth, notched round bars and single edge notched bending), the present study focuses on the circumferentially notched round bars with a notch root radius of 4mm (referred to as NT4). Figure 2 shows a sketch of the NT4 specimen and indicates its characteristic dimensions.

Materials	Plasticizer contents		Young's modulus at 0℃		Tg	
	initial	final	Before aging	After aging	Before aging	After aging
PA11	-	-	1700MPa	-	50℃	-
Aged P40	13%	6%	-	1700MPa	0℃	25℃
Aged P20R	6%	3%	-	1500MPa	-	30℃

Table 1: Physico-chemical characteristics of PA11, aged P40 and aged P20R

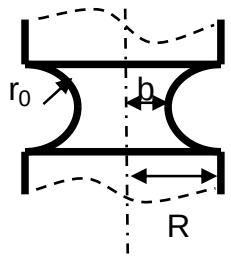

- Notch root radius : r_0 = 4mm
- Nominal radius : R = 7mm
- Minimum section radius b = 2mm
- Stress triaxiality ratio [5] maximum at the centre of the section:

$$\tau = \frac{1}{3} + \ln\left(1 + \frac{b}{2r_0}\right) \qquad (1)$$

Figure 2: Sketch and characteristic dimensions of a notched round bar

According to Bridgman [5], the NT4 specimen exhibits stress triaxiality ratio τ profile for which the maximum value is located at the centre of the minimum cross section. Equation (1) gives the expression of this initial value of τ. Note that τ also represents the part of mean stress (hydrostatic pressure) applied to the section.

NT4 specimens were tested in tension at 0℃ with two crosshead speeds of 0.05mm/s and 3mm/s respectively. During the tests the load, displacement and reduction in diameter were recorded. Each loading condition was repeated twice or three times to check the reproducibility of the test results. Some tests were interrupted before fracture in order to allow scanning electron microscope (SEM) observations of longitudinal cross-sections. Furthermore, fracture surfaces were analyzed to investigate deformation and damage mechanisms.

EXPERIMENTAL RESULTS

Mechanical response

Figure 3 illustrates plots of the net stress (σ_{net}) defined as the load divided by the net section on the first y-axis and the reduction in diameter ($(\Phi_0-\Phi)/\Phi_0$) on the second y-axis, with respect to the axial displacement. The same scale was applied to the plots for comparison

purposes. Only results at 0.05mm/s are presented here, the trends being the same at 3mm/s.

Figure 3a shows the effects of ageing by comparing the mechanical response of PA11 and aged P40. For aged P40, the peak stress is lower whereas the corresponding applied displacement is higher, compared with the PA11 curve. This is assumed to be the effect of the plasticizer added on aged P40. The displacement and reduction in diameter at failure of aged P40 (4mm and 20% respectively) are very small compared with those of PA11 (10mm and 46% respectively). Actually, aged P40 did not exhibit any extended necking zone. This drop of deformation at failure is attributed to embrittlement of aged P40 during ageing. The initial values of stiffness are similar; this confirms the Young's moduli given in Table 1.

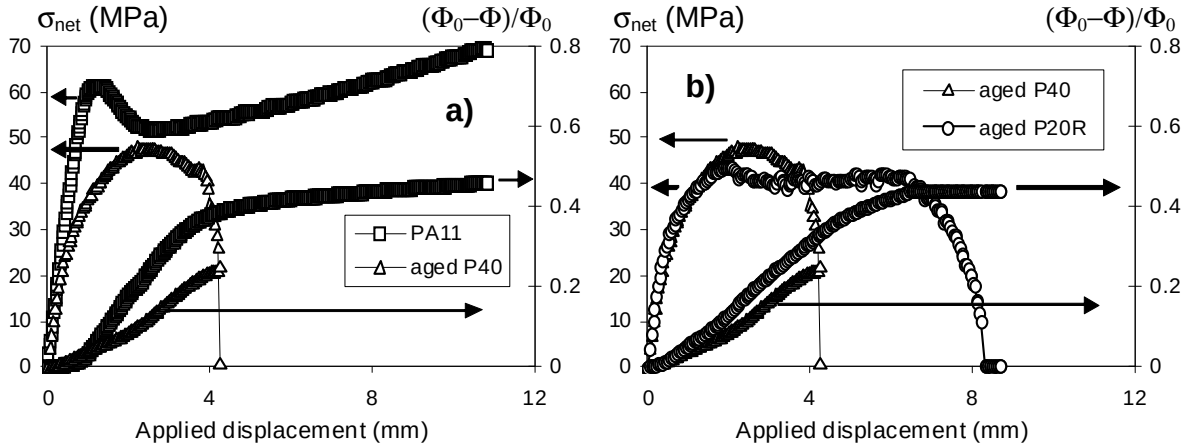

Figure 3: Net stress and diametrical reduction versus applied displacement for all PA11 materials: a) PA11 and aged P40; b) aged P40 and aged P20R

In figure 3b, aged P40 and aged P20R responses are similar at the beginning of the tests. The peak stress of aged P20R is reached sooner than that of aged P40. This may be interpreted as the net stress for which cavitation of rubber particles starts in the centre of the net section. This is then followed by extension of cavitation phenomenon towards the surface (notch root) but also by elongation of already formed voids. Displacement and reduction in diameter at failure are increased again (8mm and 45% for aged P20R). This is assumed to be a gain in ductility due to the addition of rubber particles.

Microscopic examinations

As mentioned above, some tests were arrested aiming at investigating deformation and damage mechanisms. Recall that PA11 showed voiding [6-7] during deformation, due to the presence of pre-existing voids (initial void volume fraction = 1%). The tests were stopped just before the load dropping down, at the onset of the complete failure of the specimen. The specimen was then longitudinally cut in order to observe the microstructure in the centre of the specimen. Figure 4a clearly shows a macro-crack within the aged P40 material, whereas aged P20R (fig. 4b) exhibits a homogeneous distribution in voids. Note that voids come from cavitation of rubber particles. No coalescence of these voids was detected and the porosity seems to have not yet reached a critical value.
According to these observations, final rupture of the specimen is expected to occur in two different ways:

- For aged P40, shearing and/or tearing of the remaining ligament of material between the crack and the notch root;

- For aged P20R, inter-void fibril stretching induces their hardening. As soon as a critical defect initiates the break of one fibril, the crack propagates catastrophically.

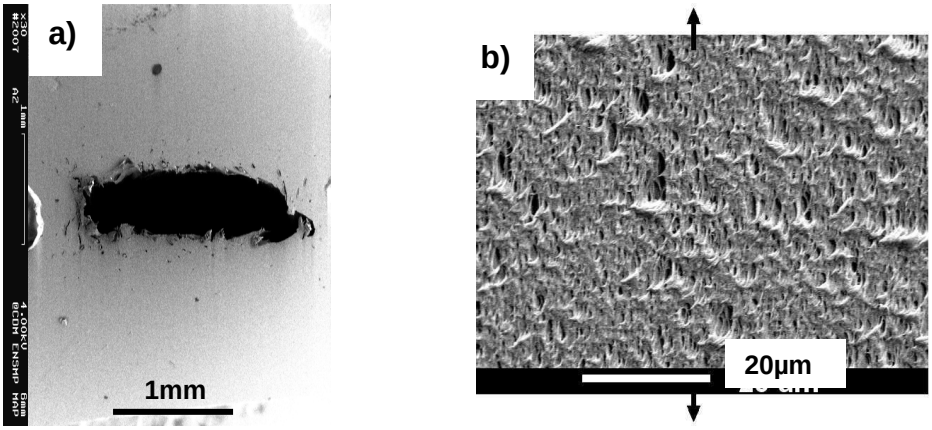

Figure 4: SEM observations of longitudinal cross-sections after tests arrested at the onset of failure: a) aged P40 presence of a macro-crack ; b) aged P20R: well dispersed voids, critical void volume fraction not reached

These two mechanisms seem to be confirmed by fracture surface examinations in figure 5. Figure 5a corresponding to aged P40 shows many dimples with some extended fibrils in the outer radius, whereas the crack initiation site is clearly shown in figure 5b (aged P20R). Fibrils are much more elongated in figure 5b than those of aged P20R in figure 5a. Indeed, fracture surface observations indicate that final rupture of aged P40 occurred in a stable way. Conversely, aged P20R specimen experienced first necking and neck extension before a final instantaneous (brittle) fracture.

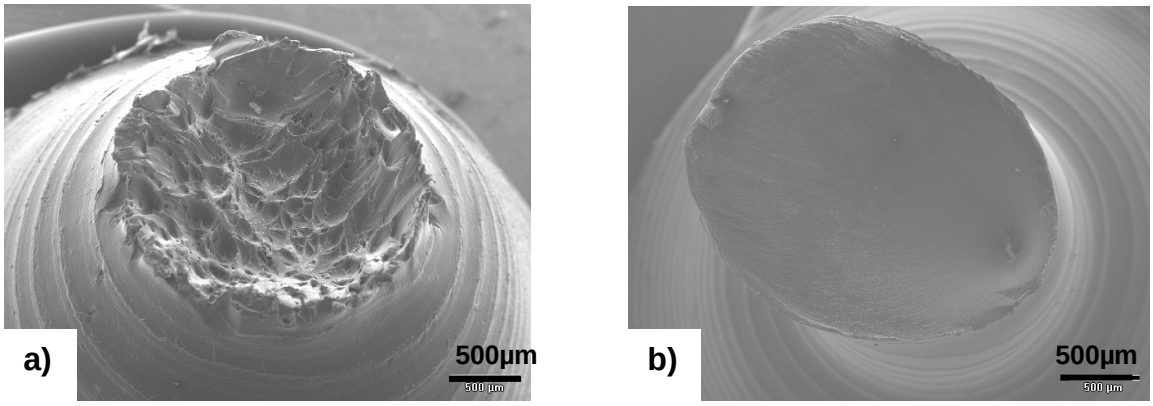

Figure 5: SEM observations of fracture surfaces: a) aged P40, diffuse ductile surface; b)aged P20R, localized crack initiation site after extended necking

DISCUSSIONS

Local approach to fracture: accounting for porosity

The materials of interest exhibit void growth during deformation. This evolution of porosity induces a volume change of the materials. The higher the stress triaxiality ratio, the higher the void growth and hence the higher the volume change and its effect on the mechanical

response of the material. Indeed a volumetric deformation has to be accounted for in a model. To this end, constitutive relationships must include a link between the mean stress and the volume change (see for instance Drucker-Prager model), in addition to the classical von Mises deviatoric criterion. Boisot [6] suggested the use of mechanics of porous media assisted by finite element analysis [8]. A modified Gurson Tvergaard Needleman [9-11] porous model was used. It was able to successfully capture the evolution of porosity as well as the location of its maximum value. Furthermore, two local failure criteria were proposed depending on the stress triaxiality ratio:

- a critical void volume fraction of about 50% for high triaxiality;
- a critical plastic strain of about 1.1 for low triaxiality.

The abovementioned observations suggest that PA11 and aged P20R follow the critical plastic strain criterion, at the end of the neck extension. Indeed neck extension decreases the triaxiality down to 0.33 (value for an uniaxial tension specimen). Conversely, aged P40 obeys a critical porosity criterion that is likely to be reached just before the stress plateau in figure 3. Detailed study of the triaxiality, porosity and the failure criteria is proposed in [6]. Note that strain rate effects can also be accounted for with the mechanics of porous media model implemented in a FE code.

Toughness

In fracture mechanics concepts, the toughness is either the critical value at failure of the stress intensity factor in LEFM, or the value at crack initiation for the J-integral for EPFM. A given material toughness can then be determined by using any pre-cracked specimen recommended by fracture mechanics theory. The area under load versus crack opening displacement curve allows the determination of the toughness, until failure for LEFM and until the peak load for EPFM respectively. For polymeric materials, it is difficult to perform these tests for several reasons such as:

- the plane strain condition is not always fulfilled; some researchers use the essential work of fracture theory, valid under plane stress condition;
- viscoelastic/viscoplastic deformation of the materials limits the use of no time dependent elasticity/plasticity constitutive relationships;
- the porosity (hence the volume change) and the high strain (finite deformation) are not correctly taken into account.

In the present study, the notch has a finite root radius (4mm) and therefore cannot be considered as sharp crack. Investigations on PA11 round bars with various notch root radii [6, 9] were already perfomed leading to many interesting conclusions. This paper introduces another parameter that, as a first approximation, can be linked to fracture toughness.

Fracture energy concepts

From figure 3, and similarly to LEFM and EPFM approaches, the area under the net stress versus applied displacement curve is representative of the total energy needed by the specimen to fracture. Additionally, although it includes both (plastic) deformation energy and cracking energy, it is similar to what is measured in impact tests such as Charpy or Izod tests. The main difference is that impact tests are done under bending stress and with dynamic conditions. Under quasi-static conditions and when test temperatures are close to T_g, impact tests might be inappropriate. Indeed if the material is tough enough, the energy of the striker may not be sufficient to break the specimen. Only large plastic strain of the specimen occurs in this case. For the three materials, areas under net stress vs. displacement curves were measured. Table 2 summarizes these fracture energies (last

column) together with other previously mentioned characteristics, in particular, the peak stress and the displacement at break that interfere in the fracture energy calculation.

Ductile and tough materials are known to have high values of fracture energy. Regarding the values in Table 2, it is shown that the fracture energy of aged P40 (160kJ/m^2) is 4 times less than that of PA11 (620kJ/m^2). Aging resulted in embrittlement of the material by reducing the strain at failure and the peak stress. Adding 3% plasticizer content in aged P40 did not compensate this embrittlement. Note that the T_g of aged P40 is 25℃ lower than that of PA11, which theoretically would have enhanced the ductility of aged P40 (test temperature 0℃ closer to the T_g of aged P40). But the shape of E' evolution clearly shows (figure1) that at 0℃ the Young's moduli are similar (typically 1700MPa).

Materials	T_g	E	Peak stress	Displ. at break	$\Delta\Phi/\Phi_0$ at break	Fracture energy
PA11	50℃	1700MPa	62MPa	10mm	46%	620±30kJ/m^2
Aged P40	25℃	1700MPa	48MPa	4mm	20%	160±10 kJ/m^2
Aged P20R	30℃	1500MPa	46MPa	8mm	45%	300±15kJ/m^2

Table 2: Values of fracture energy of PA11, aged P40 and aged P20R calculated via the net stress vs displacement curves

Improvement of fracture toughness is demonstrated with the increase in fracture energy from aged P40 (160kJ/m^2) to aged P20R (300kJ/m^2). This is mainly due to the increase in strain at failure, which is similar to that of PA11. Indeed, experimental data on aged P40 and aged P20R are quite similar in terms of peak stress and Young's modulus. Furthermore, PA11 and aged P20R curves essentially differ in the values of peak stress. Although both materials are supposed to be tough, aged P20R fracture energy is only half of that of PA11. The toughness improvement can be predicted by the length of the stress plateau (ductility) in a stress vs displacement curve as depicted in figure 3. At microscopic scale, as mentioned previously, the origin of this improvement of toughness is the homogeneous distribution of rubber particles that prevents from void coalescence during the necking process.

CONCLUSIONS

An attempt was made to characterise the ageing, plasticizing and rubber toughening effects on three grades of PA11. Once the key physico-chemical parameters of each material were presented, the specific NT4 specimen geometry was detailed. Tensile tests on this NT4 specimen were carried out. Experimental results consist of the net stress and the reduction in diameter vs. applied displacement curves. Some tests were arrested before failure of the specimens. These latter were cut longitudinally in order to perform SEM examinations of the deformation and damage (void growth) mechanisms. It was shown that aging leaded to a reduced strain at failure (embrittlement) due to the formation of a macro-crack within the material. Conversely, rubber toughened aged P20R exhibited enhanced ductility because of homogeneously distributed voids that do not coalesce. Failure of the specimen occurs after a large plateau where the necking zone extension is observed. The fracture energy parameter, corresponding to the area under the net stress vs. displacement curve was able to assess the toughness improvement thanks to the addition of rubber particles. It could be concluded that from material processing viewpoint, the toughness improvement is likely due to the good spatial distribution of rubber particles that prevents from void coalescence during the necking process.

REFERENCES

[1] Folch, L.; Burdekin, F.:
Application of coupled brittle-ductile model to study correlation between Charpy energy and fracture values.
Engineering Fracture Mechanics 63 (1999), pp. 57-80.

[2] Rossol, A.; Berdin, C., Prioul, C.:
Determination of the fracture toughness of a low alloy steel by the instrumented impact test.
International Journal of Fracture 115 (2002), pp. 205-226.

[3] Tanguy, B.; Bouchet, C.; Bugat, S.; Besson, J.:
Local approach to fracture based prediction of the ΔT_{56J} and the $\Delta T_{KIC,100}$ shifts due to irradiation for an A508 pressure vessel steel.
Engineering Fracture Mechanics 73 (2006), pp. 191-206

[4] Boisot, G. ; Fond, C.; Hochstetter, G.; Laiarinandrasana, L.:
Failure of PolyAmide 11 using a damage finite element model.
Proceedings of 17th European Conference on Fracture , 2008, September 2-5, Brno, Czech Republic.

[5] Bridgman, P. W.: 1944.
The stress distribution at the neck of a tension specimen.
Transactions ASM. 32 (1944), 553-574

[6] Boisot, G.:
Mechanisms and mechanical modelling of deformation, damage and fracture of neat and rubber-toughened PolyAmide 11.
PhD Thesis (*in French*), Ecole Nationale Supérieure des Mines de Paris 2009.

[7] Boisot, G.; Laiarinandrasana, L. ; Fond, C.; Hochstetter, G.:
The role of volume change in the ductile/brittle transition of PA11.
Proceedings of 5th ESIS TC4 conference on fracture of polymers, composites and adhesives, 2008, September 7-11, Les Diablerets, Switzerland.

[8] Besson, J.; Foerch, R.:
Large scale object-oriented finite element code design
Computer Methods in Applied Mechanics and Engineering 142 (1997), pp. 165-187

[9] Gurson, A.L.:
Continuum theory of ductile rupture by void nucleation and growth: Part 1 yield criteria and flow rules for porous ductile media.
J. Eng. Mater Technol. 99 (1977), pp. 2-15.

[10] Tvergaard, V., Needleman, A.:
Analysis of the cup-cone fracture in a round tensile bar.
Acta Metall. 32 (1984), pp. 157-169.

[11] Laiarinandrasana, L.; Besson, J.; Lafarge, M.; Hochstetter, G.:
Temperature-dependent mechanical behaviour of PVDF: Experiments and numerical modelling.
International Journal of Plasticity 25(7) (2009), pp. 1301-1324.

Corresponding author: lucien.laiarinandrasana@mines-paristech.fr